# Cascaded fiber-optic Fabry-Perot interferometers with Vernier effect for highly sensitive measurement of axial strain and magnetic field

Zhang, Peng; Tang, Ming; Gao, Feng; Zhu, Benpeng; Fu, Songnian; Ouyang, Jun; Shum, Perry Ping; Liu, Deming

2014

Zhang, P., Tang, M., Gao, F., Zhu, B., Fu, S., Ouyang, J., et al. (2014). Cascaded fiber-optic Fabry-Perot interferometers with Vernier effect for highly sensitive measurement of axial strain and magnetic field. Optics express, 22(16), 19581-19588.

https://hdl.handle.net/10356/79617

https://doi.org/10.1364/OE.22.019581

# Cascaded fiber-optic Fabry-Perot interferometers with Vernier effect for highly sensitive measurement of axial strain and magnetic field

**Peng Zhang,[1,2] Ming Tang,[1,2,*] Feng Gao,[1,2] Benpeng Zhu,[2] Songnian Fu,[1,2] Jun Ouyang,[2] Perry Ping Shum,[3] and Deming Liu,[1,2]**

[1] *Wuhan National Laboratory for Optoelectronics, Huazhong University of Science and Technology, Wuhan, 430074, China*

[2] *National Engineering Laboratory for Next Generation Internet Access System, School of Optics and Electronic Information, Huazhong University of Science and Technology, Wuhan, 430074, China*

[3] *Photonics Centre of Excellence, School of Electrical and Electronic Engineering, Nanyang Technological University, 637553, Singapore*

[*] *tangming@mail.hust.edu.cn*

**Abstract:** We report a highly sensitive fiber-optic sensor based on two cascaded intrinsic fiber Fabry-Perot interferometers (IFFPIs). The cascaded IFFPIs have different free spectral ranges (FSRs) and are formed by a short section of hollow core photonic crystal fiber sandwiched by two single mode fibers. With the superposition of reflective spectrum with different FSRs, the Vernier effect will be generated in the proposed sensor and we found that the strain sensitivity of the proposed sensor can be improved from 1.6 pm/με for a single IFFPI sensor to 47.14 pm/με by employing the Vernier effect. The sensor embed with a metglas ribbon can be also used to measure the magnetic field according to the similar principle. The sensitivity of the magnetic field measurement is achieved to be 71.57 pm/Oe that is significantly larger than the 2.5 pm/Oe for a single IFFPI sensor.



**OCIS codes:** (060.2370) Fiber optics sensors; (120.2230) Fabry-Perot; (120.3180) Interferometry; (230.3810) Magneto-optic systems; (280.4788) Optical sensing and sensors.

## References and links

1. D. Wu, T. Zhu, G. Y. Wang, J. Y. Fu, X. G. Lin, and G. L. Gou, "Intrinsic fiber-optic Fabry-Perot interferometer based on arc discharge and single-mode fiber," Appl. Opt. **52**(12), 2670–2675 (2013).
2. Q. Shi, F. Y. Lv, Z. Wang, L. Jin, J. J. Hu, Z. Y. Liu, G. Y. Kai, and X. Y. Dong, "Environmentally stable Fabry–Pérot-type strain sensor based on hollow-core Photonic bandgap fiber," IEEE Photon. Technol. Lett. **20**(4), 237–239 (2008).
3. D. J. J. Hu, Y. X. Wang, J. L. Lim, T. S. Zhang, K. B. Milenko, Z. H. Chen, M. Jiang, G. H. Wang, F. Luan, P. P. Shum, Q. Z. Sun, H. F. Wei, W. J. Tong, and T. R. Wolinski, "Novel miniaturized Fabry–Perot refractometer based on a simplified hollow-core fiber with a hollow silica sphere Tip," IEEE Sens. J. **12**(5), 1239–1245 (2012).
4. J. J. Tian, Y. J. Lu, Q. Zhang, and M. Han, "Microfluidic refractive index sensor based on an all-silica in-line Fabry-Perot interferometer fabricated with microstructured fibers," Opt. Express **21**(5), 6633–6639 (2013).
5. Y. Zhao, R. Q. Lv, Y. Ying, and Q. Wang, "Hollow-core photonic crystal fiber Fabry–Perot sensor for magnetic field measurement based on magnetic fluid," Opt. Laser Technol. **44**(4), 899–902 (2012).
6. O. Frazão, S. H. Aref, J. M. Baptista, J. L. Santos, H. Latifi, F. Farahi, J. Kobelke, and K. Schuster, "Fabry–Pérot cavity based on a suspended-core fiber for strain and temperature measurement," IEEE Photon. Technol. Lett. **21**(17), 1229–1231 (2009).
7. D. X. Dai, "Highly sensitive digital optical sensor based on cascaded high-Q ring-resonators," Opt. Express **17**(26), 23817–23822 (2009).
8. L. Jin, M. Y. Li, and J. J. He, "Highly-sensitive optical sensor using two cascaded-microring resonators with Vernier effect," in Asia Communications and Photonics Conference, Technical Digest (TD), (Optical Society of America, 2009), paper TuM4.

#212943 - $15.00 USD Received 28 May 2014; revised 5 Jul 2014; accepted 24 Jul 2014; published 6 Aug 2014

9. T. Claes, W. Bogaerts, and P. Bienstman, "Experimental characterization of a silicon photonic biosensor consisting of two cascaded ring resonators based on the Vernier-effect and introduction of a curve fitting method for an improved detection limit," Opt. Express **18**(22), 22747–22761 (2010).
10. L. Jin, M. Y. Li, and J. J. He, "Analysis of wavelength and intensity interrogation methods in cascaded double-ring sensors," J. Lightwave Technol. **30**(12), 1994–2002 (2012).
11. L. Jin, M. Y. Li, and J. J. He, "Optical waveguide double-ring sensor using intensity interrogation with a low-cost broadband source," Opt. Lett. **36**(7), 1128–1130 (2011).
12. P. Russell, "Photonic crystal fibers," Science **299**(5605), 358–362 (2003).
13. A. D. Kersey, M. A. Davis, H. J. Patrick, M. LeBlanc, K. P. Koo, C. G. Askins, M. A. Putnam, and E. J. Friebele, "Fiber grating sensors," J. Lightwave Technol. **15**(8), 1442–1463 (1997).
14. F. C. Favero, L. Araujo, G. Bouwmans, V. Finazzi, J. Villatoro, and V. Pruneri, "Spheroidal Fabry-Perot microcavities in optical fibers for high-sensitivity sensing," Opt. Express **20**(7), 7112–7118 (2012).
15. P. Zu, C. C. Chan, W. S. Lew, L. M. Hu, Y. X. Jin, H. F. Liew, L. H. Chen, W. C. Wong, and X. Y. Dong, "Temperature-insensitive magnetic field sensor based on nanoparticle magnetic fluid and photonic crystal fiber," IEEE Photon. J. **4**(2), 490–498 (2012).
16. L. Gao, T. Zhu, M. Deng, K. S. Chiang, X. K. Sun, X. P. Dong, and Y. S. Hou, "Long-period fiber grating within D-shaped fiber using magnetic fluid for magnetic-field detection," IEEE Photon. J. **4**(6), 2094–2104 (2012).
17. H. T. Savage and M. L. Spanot, "Theory and application of highly magnetoelastic Metglas 2605SC," J. Appl. Phys. **53**(11), 8092–8097 (1982).

## 1. Introduction

In the past few decades, the intrinsic fiber Fabry-Perot interferometers (IFFPIs) sensor have been widely studied for their physical, chemical and biological sensing applications, such as temperature, strain, and refractive index (RI), due to their simple and compact structure, good stability, and high resolution. So far, several techniques have been introduced to form the IFFPI sensor, such as internal film coating, fiber Bragg grating, laser irradiated points, chemical etching, focused ion beam techniques, and refractive-index mismatch between two fibers in the splicing joint [1], etc. Recently, Hollow core fiber (HCF)-based IFFPI that utilize the RI mismatch between the air core of HCF and the glass core of solid core fiber have attracted extensive interest because it is easy to prepare with compact size. The IFFPI based on HCF have been developed for the measurement of axial strain [2], temperature [3], refractive index [4], and magnetic field [5], respectively. For an IFFPI sensor, when the cavity length changes, the resonant wavelength of the IFFPI will shift. In order to monitor the change in cavity length of IFFPI, one simple way for sensing is to measure the shift of the resonance wavelength using an optical spectrum analyzer (OSA) with a very high resolution [6].

The Vernier effect has been employed by Vernier Caliper to enhance the accuracy of length measurement. An optical sensor applying the Vernier effect to sense the refractive index is reported in 2009 [7, 8]. The optical sensor consists of two cascaded rings and can obtain ultra-high sensitivity due to the Vernier effect by implementing wavelength interrogation. However, the smallest detectable shift and detection limit of the optical sensor is limited. In [9] and [10], a curve fitting method and intensity interrogation method that compare the amplitude of the major and the adjacent peak are introduced for improving the detection limit of wavelength interrogation system for this kind of optical sensor. In [11], through interrogating the optical intensity from the optical sensor output port, a two cascaded rings-based RI sensor with a low-cost broadband source is implemented to avoid the use of expensive device and reduce the cost of the wavelength interrogation system. However, the fabrication process of micro-rings based resonator using silicon-on-insulator technology is sophisticated and expensive. Besides that, the optical coupling between the micro-rings resonator and optical fiber is difficult due to the large mode field mismatch between them. In order to take full advantage of the Vernier effect, a periodic spectrum with dip or peak having the same amplitude is favorable. As is well known, the spectrum of the IFFPI meets the criteria. The all-fiber structured IFFPI is also beneficial to the sensing application due to its compatibility with fiber-optic measurement system.

In this paper, we propose a fiber-optic sensor based on two cascaded IFFPIs with different FSRs. One of the two IFFPIs is fixed on a micro-moving platform as the sensing head for strain measurement or a piece of metglas ribbon for magnetic field measurement, and the other one is

#212943 - $15.00 USD Received 28 May 2014; revised 5 Jul 2014; accepted 24 Jul 2014; published 6 Aug 2014

free to form a reference IFFPI. Due to their different FSRs, the reflection spectrum of the proposed sensor will have a major dip and some minor dips. When the cavity length of the sensing IFFPI increases, the major dip shifts discretely and the shift of the major peak is equal to multiple FSRs of the reference IFFPI. This is so-called the Vernier effect. We also introduce a curve fitting method for realizing a continuous measurement of strain or magnetic field. In this way, we have established a fiber-optic sensor with a high sensitivity that is many times higher than that of a single IFFPI sensor.

## 2. Sensor structure and operation principle

Two IFFPIs, i.e., sensing and reference IFFPI, were cascaded by a long section of SMF to form a high sensitive fiber-optic sensor, as shown in Fig. 1(a). The FSRs of sensing and reference IFFPI $\Delta\lambda_{FSR_S}$, $\Delta\lambda_{FSR_R}$ are designed to be slightly different to employ the Vernier effect, which could be realized by choosing different cavity length ($L_S$ and $L_R$) for sensing and reference IFFPI. The IFFPI are formed by a short section of hollow core photonic crystal fiber (HC-PCF), as shown in Fig. 1(b), sandwiched by two single mode fibers (SMFs). When the SMF was spliced with the HC-PCF, the air-glass interface will be formed in the light path. Because of the Fresnel reflection generating at the air-glass interface due to the RI mismatch, a small part of light will be reflected at the interface, while a great part of light will transmit. So the light pass through the sensing and reference IFFPI through the lead-in fiber and connecting fiber successively. Meanwhile, the interferometric spectrum reflected from the sensing and reference IFFPI will encounter and superimpose at the lead-in fiber.

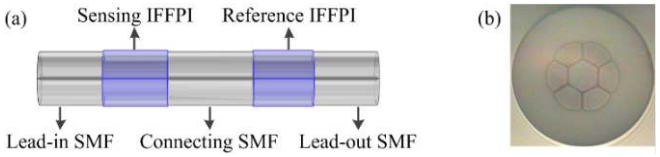


Fig. 1. (a) The schematic configuration of the present optical sensor based on cascaded IFFPI; (b) The optical microscopic image of the HC-PCF cross-section structure

In order to understand the reflection spectrum of the IFFPI based on the HC-PCF, we investigated the mode field distribution of the HC-PCF and SMF by the finite element simulation environment (Comsol 4.4), as shown in Figs. 2. From Figs. 2, we can know the mode field of the HC-PCF is larger than that of the SMF at 1500nm. Because of this, the coupling loss between them will be large. Thus we can simplify the reflection spectrum as consequence of dual-beam interference. The reflection spectrum of the sensing and reference IFFPI can be expressed as $R_S = a\cos(4\pi L_S n/\lambda)$ and $R_R = a\cos(4\pi L_R n/\lambda)$, where $a$ is the amplitude of the reflection spectrum of single IFFPI, and $n$ is the effective index of the fundamental mode of the HC-PCF.

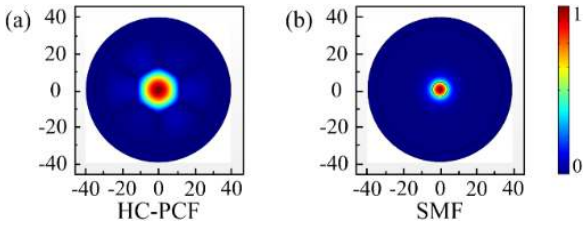


Fig. 2. The fundamental mode field of the HC-PCF (a) and SMF (b) at 1500 nm.

In order to describe the Vernier principle of the proposed sensor, the reflection spectrum $R_R$ and $R_S$ of the reference and sensing IFFPI are plotted in Fig. 3(a) and 3(b), respectively.

#212943 - $15.00 USD Received 28 May 2014; revised 5 Jul 2014; accepted 24 Jul 2014; published 6 Aug 2014

Both reference and sensing IFFPIs have a series of resonant wavelengths $\lambda_{R(i)}$ and $\lambda_{S(j)}$. In the proposed sensor, we choose $L_R < L_S$, so that $\Delta\lambda_{FSR_R}$ is larger than $\Delta\lambda_{FSR_S}$. When the *i*-th resonance wavelength $\lambda_{R(i)}$ of reference IFFPI is coincided with the *j*-th resonance wavelength $\lambda_{S(j)}$ of sensing IFFPI, the reflection spectrum $R_C$ has a common resonance wavelength $\lambda_{C(i)}$. While the adjacent resonance wavelengths $\lambda_{R(i+1)}$ and $\lambda_{S(j+1)}$ are separated because $\Delta\lambda_{FSR_R}$ is not equal to $\Delta\lambda_{FSR_S}$, consequently the amplitude of the adjacent dip is smaller than the common resonance. Because of their different FSRs, the reflection spectrum of the proposed sensor will have a series of dips with different amplitude that will form a periodic envelope function, as shown in Fig. 3(c). The envelope function consisting of the dips can be expressed by

$$R_C = 2a\cos\left[\frac{2\pi\left(L_R - L_S\right)n}{\lambda}\right]. \tag{1}$$

And the period $\Delta\lambda_{FSR_C}$ of the envelop function is given by

$$\Delta\lambda_{FSR_C} = \frac{\Delta\lambda_{FSR_R}\Delta\lambda_{FSR_S}}{\left|\Delta\lambda_{FSR_R} - \Delta\lambda_{FSR_S}\right|}. \tag{2}$$

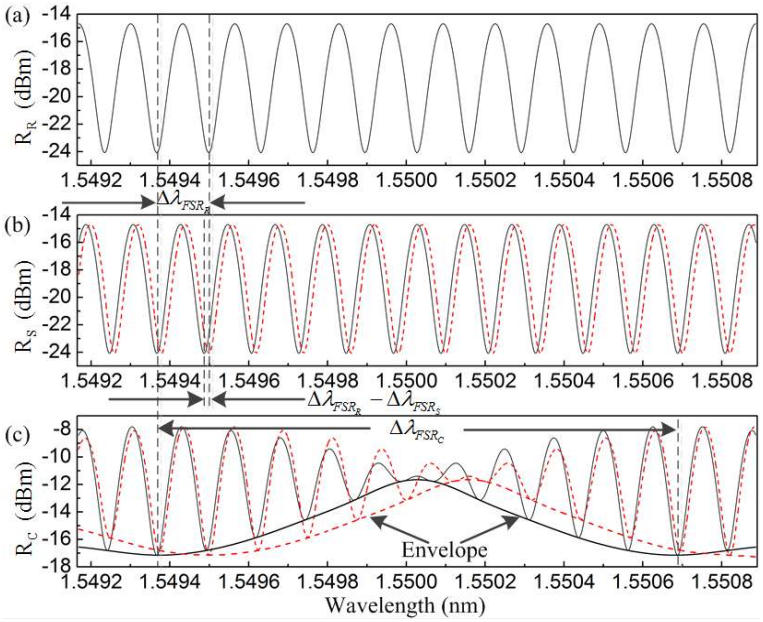


Fig. 3. (a) Reflection spectrum of reference IFFPI; (b) Reflection spectrum of sensing IFFPI before (black solid line) and after (red dashed line) elongating; (c) Reflection spectrum of the proposed sensor before (black solid line) and after (red dashed line) the sensing IFFPI is elongating.

When the cavity length of the IFFPI *L* changes, the resonant wavelength of the IFFPI $\lambda_{(i)}$ changes accordingly, i.e.

$$\Delta\lambda = \lambda_{(i)}\left(\frac{\Delta n}{n} + \frac{\Delta L}{L}\right), \tag{3}$$

#212943 - $15.00 USD Received 28 May 2014; revised 5 Jul 2014; accepted 24 Jul 2014; published 6 Aug 2014

where $\Delta n$ and $\Delta L$ are the strain-induced change in effective index of the fundamental mode and cavity length of the HC-PCF in IFFPI, respectively [2]. When cavity length of the sensing IFFPI changes slightly, $\Delta n$ can be ignored through the analysis did by the software of finite element analysis. Equation (3) can be rewritten as $\Delta\lambda = \lambda_{(i)}\Delta L/L$. So when the cavity length of the sensing IFFPI $L_S$ changes, the shift of its resonant wavelength is

$$\Delta\lambda_S = \lambda_{S(i)}\frac{\Delta L_S}{L_S}, \tag{4}$$

where $\Delta L_S$ is the strain-induced change in cavity length of the sensing IFFPI. Since the reference IFFPI is free, the resonant wavelength of the reference IFFPI $\lambda_{R(i)}$ will be unchanged. Consequently the resonant wavelengths $\lambda_{S(i)}$ and $\lambda_{R(j)}$ become separated while the adjacent resonance wavelengths $\lambda_{S(i+1)}$ and $\lambda_{R(j+1)}$ become close. When the length of the sensing IFFPI increases further, the adjacent resonant wavelengths $\lambda_{S(i+1)}$ and $\lambda_{R(j+1)}$ become coincided and the common resonant wavelength jumps to the wavelength $\lambda_{R(i+1)}$, as shown by the red dotted curve in Fig. 3(b). When the cavity length of sensing IFFPI increases further, the major peak will jump to the next resonant wavelength of reference IFFPI. From the Fig. 3(c), we can see that the envelop function of the spectrum reflected from the proposed sensor also shift to the long wavelength direction that is the same as the resonance wavelength shift of the sensing IFFPI. In this way, when the change in cavity length of sensing IFFPI is $\Delta L_S$, the shift of the common resonance wavelength, i.e., the valley of the envelop function, is given by

$$\Delta\lambda_C = \lambda_{S(i)}\bullet\frac{\Delta L_S}{L_S}\bullet\frac{\Delta\lambda_{FSR_R}}{\left|\Delta\lambda_{FSR_R}-\Delta\lambda_{FSR_S}\right|}. \tag{5}$$

Compared to the shift of a single IFFPI, the shift of the cascaded IFFPI sensor is magnified by a factor of

$$M = \frac{\Delta\lambda_{FSR_R}}{\left|\Delta\lambda_{FSR_R}-\Delta\lambda_{FSR_S}\right|}. \tag{6}$$

If we simply sense the physical quantity through the resonant wavelength with maximal amplitude, the minimal detectable wavelength $\Delta\lambda_{\min}$ is $\Delta\lambda_{FSR_R}$, corresponding to the change in cavity length of the sensing IFFPI of $\Delta L_S = L_S\left|\Delta\lambda_{FSR_R}-\Delta\lambda_{FSR_S}\right|/\lambda_{S(i)}$. This will severely restrict the resolution of the proposed sensor. Therefore we choose the curve fitting method introduced by Tom Claes in [9] for an improved detection limit. This method not only improve the resolution but also reduce the measuring error introduced by power jitter and multimode interference.

### 3. Sensor design and fabrication

To implement the IFFPI, we employ the RI mismatch between the air core of HC-PCF and the glass core of solid core fiber at the joint of the HC-PCF and SMF to generate Fresnel reflectivity as the reflecting mirror of the IFFPI. Figure 1(b) shows the microscopic cross section of the HC-PCF, which is fabricated by Yangtze Optical Fiber and Cable Company Ltd. The fiber has an air core surrounded by a ring of thin silica wall. Light can be guided in the air core due to the antiresonance between the core mode and the modes of the inner silica wall [12]. In the process of IFFPI-fabrication, at first, the HC-PCF was cleaved and spiced with the SMF. After cleaving the HC-PCF side of the HC-PCF-SMF structure at a desired HC-PCF length,

#212943 - $15.00 USD Received 28 May 2014; revised 5 Jul 2014; accepted 24 Jul 2014; published 6 Aug 2014

another section of SMF was spliced together. Whereafter, another IFFPI that has slightly different cavity length was fabricated in the same way. Finally, the two IFFPIs were connected by a long section of SMF. The arc fusion parameters used to splice SMF and HC-PCF including arc duration and strength have been optimized to obtain higher extinction ratio.

The cavity length of the sensing and reference IFFPIs we obtained are 9.724 mm and 9.389 mm, corresponding to FSRs of 0.1235 nm and 0.1279 nm, respectively. In this case, the amplification factor $M$ = 28.94 can be obtained from Eq. (6). And the FSR of two cascaded IFFPIs sensor is calculated as $\Delta\lambda_{FSR_C} = 3.57nm$ according to Eq. (2).

## 4. Experimental results and discussions

To analyze the performance and sensing properties of the proposed sensor, we launched light to the two cascaded IFFPIs from a broadband source through a fiber optic circulator, as sketched in Fig. 4. The reflected light was fed to an optical spectrum analyzer. Figures 5 show the representative reflection spectrum of the proposed sensor and its measured FSR matches the theoretical result very well. From the Fig. 5(a), we can see that the reflection spectrum has obvious periodicity. And the amplitude of the lower valleys is larger than that of the upper peaks, so we choose the shift of the lower valley as the sensing indicator. The enlarged view of one of the valleys is shown in Fig. 5(b). It is clearly that the lower valleys consist of a series of dips with different amplitude.

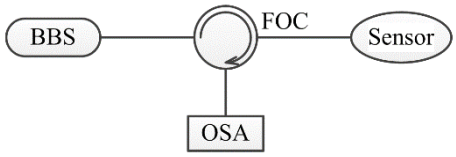


Fig. 4. Schematic of the experimental setup. BBS stands for broadband optical source; OSA stands for optical spectrum analyzer; FOC stands for fiber optic circulator.

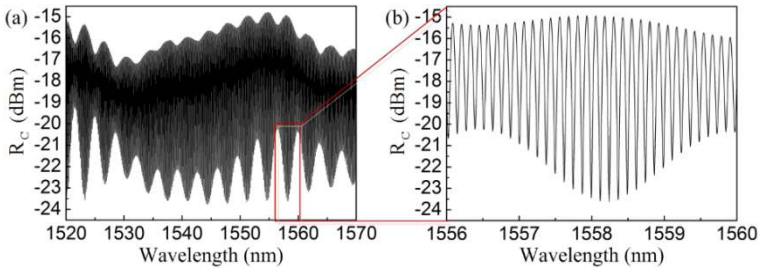


Fig. 5. (a) The response of the output port of the cascaded IFFPIs in the broad band; (b) the enlarged view for the valley.

First, the proposed sensor was tested as a sensor for the strain measurement. The sensing IFFPI was fixed on a micro-moving platform as the sensing element, while the reference IFFPI is free as the reference element. The micro-moving platform fabricated by Throlabs, lnc. has the resolution of 50 nm. We measure the strain response of the sensor from 0 to 200 $\mu\varepsilon$ with a step of 10 $\mu\varepsilon$.

In Fig. 6(a), we show the amplitudes of all the dips (locating at different resonance wavelengths of the reference IFFPI) with different strain applied. It is clear that the output spectrum was found to be red shifted with the increase of the strain. As mentioned above, we employ the curve fitting method given by Eq. (1) to get more accurate results and improve resolution. The color curves shown in Fig. 6(a) are the lower fitting envelope function $R_E$. The wavelength corresponding to the valley of the fitting envelope function observed as a function of strain in sensor is shown as in Fig. 6(b), and a good linearity is observed. This linear result is in consistent with the aforementioned theoretical analysis. The wavelength shifts about 0.5 nm

#212943 - $15.00 USD Received 28 May 2014; revised 5 Jul 2014; accepted 24 Jul 2014; published 6 Aug 2014

was achieved when there is a strain-change of $\Delta\varepsilon=10\times10^{-6}$. This gives a high sensitivity of about 47.14 pm/με, which is about 29 times higher than the sensitivity of a single IFFPI-based sensor. The magnification factors obtained from experiment and theoretical analysis are quite close. The strain sensitivity of our sensor is 50 times higher than that of an FBG-based technique [13]. The strain sensitivity is also about five times higher than that of strain sensors based on microbubble [14].

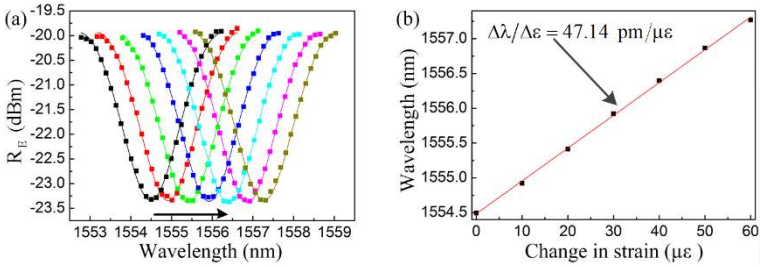


Fig. 6. As the strain-change increases, (a) the amplitude of all the dips locating at different resonance wavelengths and the fitting envelope curve according to Eq. (1); (b) the wavelength corresponding to the dip of the envelope function.

In order to sense the magnetic field intensity, the sensing IFFPI was sandwiched with two slices of metglas ribbon and fixed by epoxy. When applying magnetic field to the sensor, the metglas ribbon will distort to a certain displacement due to the magnetostrictive effect, and the cavity length of IFFPI sandwiched with two slices of metglas ribbon will also changes. The measurement principle of the magnetic field is similar to that of the strain measurement for the proposed sensor. The only difference is the reason causing the change in cavity length of the sensing IFFPI. It is the mechanical force for the strain measurement and is the magnetic field for the magnetic measurement.

We experimentally measured the reflection spectrum of the proposed sensor under magnetic field intensity from 0 to 50 Oe with a step with 1 Oe. The curve-fitted envelope of the reflection spectrum $R_E$ under different magnetic field is shown in Fig. 7(a). From the Fig. 7(a), we can see that the output spectrum will shift to a longer wavelength with the increase of the magnetic field intensity. With the increasing of the magnetic field intensity, the cavity length of sensing IFFPI will be increased due to the metglas ribbon attached to the HC-PCF because of the magnetostrictive effect. The relationship of magnetic field intensity versus one of the dip could be obtained by tracing the shifts of the specific dip as shown in Fig. 7(b), from which a maximum sensitivity about 71.57 pm/Oe of magnetic intensity measurement could be obtained. The magnetic field sensitivity is relatively improved compared with some magnetic field sensors based on magnetic fluid [5] [15] [16]. It is obvious that the relationship between detected dip wavelength and magnetic field is nonlinear. This is mainly caused by the inherent nonlinear response of the strain in metglas ribbon to the applied magnetic field intensity [17]. Although the relationship of strain to the dip wavelength shift of the cascaded IFFPI sensor is linear, the relationship between the wavelength and magnetic field intensity would still be nonlinear. A linear detection range between 20 and 35 Oe has been achieved in this report. The sensitivity and linear detection range of the proposed fiber magnetic sensor are mainly determined by the property of the magnetostriction materials. We can improve the performance of the proposed sensor by improving the property of metglas or choosing other kind of magnetostriction materials with better performance.

#212943 - $15.00 USD Received 28 May 2014; revised 5 Jul 2014; accepted 24 Jul 2014; published 6 Aug 2014

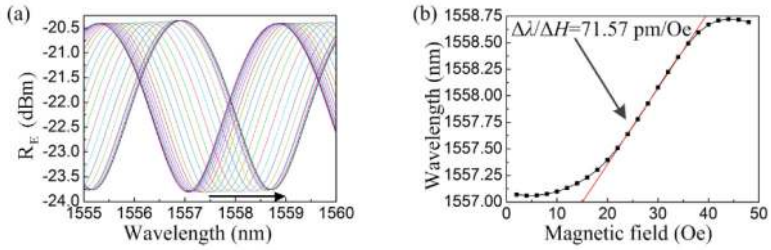


Fig. 7. (a) The fitting envelope curve according to Eq. (1); (b) The wavelength of the dip as a function of the magnetic field intensity.

From the Fig. 6(a) and Fig. 7(a), we can see that the extinction ratio of the envelope shape is not very high. This is mainly caused by the coupling loss due to the mode field mismatch between the HC-PCF and SMF. When injected into lead-in fiber, the light reflected from the reference IFFPI undergoes higher loss. Therefore, large intensity difference between the light reflected from two IFFPIs will be generated. In addition, the HC-PCF also introduces modal interferences. A HC-PCF with mode field distribution similar with SMF will be useful to reduce the coupling loss hence improve the performance of the proposed sensor.

## 5. Conclusion

In summary, we have proposed a fiber-optic sensor based on cascaded IFFPIs. The characteristics of the sensor have been theoretically analyzed. One of the two IFFPIs is fixed on a micro-moving platform or a piece of metglas ribbon for strain or magnetic field measurement, and the other one is free. The two cascaded IFFPIs have different FSRs and consequently the envelope of spectrum reflected from the proposed sensor will have periodicity. When the shift in the resonant wavelength of the sensing IFFPI is $\Delta\lambda_{FSR_R} - \Delta\lambda_{FSR_S}$, the shift in the valley of envelop is $\Delta\lambda_{FSR_R}$. Therefore, the fiber-optic sensor has a high sensitivity which is *M* times higher than that of a single IFFPI. Through the curve fitting method, we realized continuous measurements of strain and magnetic field. The strain and magnetic field sensitivity of the sensor are as large as 47.14 pm/με and 71.57 pm/Oe by employing the Vernier effect, respectively.

## Acknowledgments

The work presented in this paper is supported by the 863 High Technology Plan of China (2013AA013402), the National Natural Science Foundation of China (NSFC) under Grant No. 61107087 and 61331010, the Fundamental Research Funds for the Central Universities', HUST: 2013TS052, and the Program for New Century Excellent Talents in University (NCET-13-0235). The authors would like to extend their appreciation to Dr. Weijun Tong and Dr. Huifeng Wei for their support to this work.

#212943 - $15.00 USD Received 28 May 2014; revised 5 Jul 2014; accepted 24 Jul 2014; published 6 Aug 2014